Editors' Suggestion | Featured in Physics

Filamentation of a relativistic proton bunch in plasma

L. Verra[1,*] C. Amoedo,[1] N. Torrado,[1,2] A. Clairembaud,[1,3] J. Mezger,[4] F. Pannell,[5] J. Pucek,[4] N. van Gils,[1] M. Bergamaschi,[4] G. Zevi Della Porta,[1,4] N. Lopes,[2] A. Sublet,[1] M. Turner,[1] E. Gschwendtner,[1] and P. Muggli[4]
(AWAKE Collaboration)

R. Agnello,[6] C. C. Ahdida,[1] Y. Andrebe,[6] O. Apsimon,[7,8] R. Apsimon,[8,9] J. M. Arnesano,[1] V. Bencini,[1,10] P. Blanchard,[6] P. N. Burrows,[10] B. Buttenschön,[11] A. Caldwell,[4] M. Chung,[12] D. A. Cooke,[5] C. Davut,[7,8] G. Demeter,[13] A. C. Dexter,[8,9] S. Doebert,[1] J. Farmer,[4] A. Fasoli,[6] R. Fonseca,[14,2] I. Furno,[6] E. Granados,[1] M. Granetzny,[15] T. Graubner,[16] O. Grulke,[11,17] E. Guran,[1] J. Henderson,[8,18] M. Á. Kedves,[13] F. Kraus,[16] M. Krupa,[1] T. Lefevre,[1] L. Liang,[7,8] S. Liu,[19] K. Lotov,[20,21] M. Martinez Calderon,[1] S. Mazzoni,[1] K. Moon,[12] P. I. Morales Guzmán,[4] M. Moreira,[2] T. Nechaeva,[4] N. Okhotnikov,[20,21] C. Pakuza,[10] A. Pardons,[1] K. Pepitone,[22] E. Poimendidou,[1] A. Pukhov,[23] R. L. Ramjiawan,[1,10] L. Ranc,[4] S. Rey,[1] R. Rossel,[1] H. Saberi,[7,8] O. Schmitz,[15] E. Senes,[1] F. Silva,[24] L. Silva,[2] B. Spear,[10] C. Stollberg,[6] C. Swain,[8,25] A. Topaloudis,[1] P. Tuev,[20,21] F. Velotti,[1] V. Verzilov,[19] J. Vieira,[2] E. Walter,[26] C. Welsch,[8,25] M. Wendt,[1] M. Wing,[5] J. Wolfenden,[8,25] B. Woolley,[1] G. Xia,[8,7] V. Yarygova,[20,21] and M. Zepp[15]

[1]*CERN, 1211 Geneva 23, Switzerland*
[2]*GoLP/Instituto de Plasmas e Fusão Nuclear, Instituto Superior Técnico, Universidade de Lisboa, 1049-001 Lisbon, Portugal*
[3]*Université Paris-Saclay, CNRS-IN2P3, IJCLab 91898 Orsay, France*
[4]*Max Planck Institute for Physics, 80805 Munich, Germany*
[5]*UCL, London WC1 6BT, United Kingdom*
[6]*Ecole Polytechnique Federale de Lausanne (EPFL), Swiss Plasma Center (SPC), 1015 Lausanne, Switzerland*
[7]*University of Manchester, Manchester M13 9PL, United Kingdom*
[8]*Cockcroft Institute, Warrington WA4 4AD, United Kingdom*
[9]*Lancaster University, Lancaster LA1 4YB, United Kingdom*
[10]*John Adams Institute, Oxford University, Oxford OX1 3RH, United Kingdom*
[11]*Max Planck Institute for Plasma Physics, 17491 Greifswald, Germany*
[12]*UNIST, Ulsan 44919, Republic of Korea*
[13]*HUN-REN Wigner Research Centre for Physics, 1121 Budapest, Hungary*
[14]*ISCTE - Instituto Universitéario de Lisboa, 1049-001 Lisbon, Portugal*
[15]*University of Wisconsin, Madison, Wisconsin 53706, USA*
[16]*Philipps-Universität Marburg, 35032 Marburg, Germany*
[17]*Technical University of Denmark, 2800 Kongens Lyngby, Denmark*
[18]*STFC/ASTeC, Daresbury Laboratory, Warrington WA4 4AD, United Kingdom*
[19]*TRIUMF, Vancouver BC V6T 2A3, Canada*
[20]*Budker Institute of Nuclear Physics SB RAS, 630090 Novosibirsk, Russia*
[21]*Novosibirsk State University, 630090 Novosibirsk, Russia*
[22]*Angstrom Laboratory, Department of Physics and Astronomy, 752 37 Uppsala, Sweden*
[23]*Heinrich-Heine-Universität Düsseldorf, 40225 Düsseldorf, Germany*
[24]*INESC-ID, Instituto Superior Técnico, Universidade de Lisboa, 1049-001 Lisbon, Portugal*
[25]*University of Liverpool, Liverpool L69 7ZE, United Kingdom*
[26]*Max Planck Institute for Plasma Physics, 80805 Munich, Germany*

(Received 21 December 2023; accepted 25 March 2024; published 7 May 2024)

We show in experiments that a long, underdense, relativistic proton bunch propagating in plasma undergoes the oblique instability, which we observe as filamentation. We determine a threshold value for the ratio between the bunch transverse size and plasma skin depth for the instability to occur. At the threshold, the outcome of the experiment alternates between filamentation and self-modulation instability (evidenced by longitudinal modulation into microbunches). Time-resolved images of the bunch density distribution reveal that filamentation grows to an observable level late along the bunch, confirming the spatiotemporal nature of the instability. We provide a rough estimate of the amplitude of the magnetic field generated in the plasma by the instability and show that the associated magnetic energy increases with plasma density.

DOI: 10.1103/PhysRevE.109.055203

[*]Present address: INFN Laboratori Nazionali di Frascati, 00044 Frascati, Italy; livio.verra@lnf.infn.it

I. INTRODUCTION

When a perturbation is introduced in a plasma, e.g., by a streaming relativistic, charged particle bunch, plasma electrons move to restore the charge and current neutrality of the system. Compensation of the space-charge field of the bunch can cause oscillatory phenomena such as plasma wakefields [1]. Depending on the bunch spatial dimensions, compared to the physical quantities (e.g., plasma wave number and skin depth) determining the unstable modes, the bunch-plasma system can be prone to different instability regimes [2,3].

When the root-mean-square (rms) length of the bunch σ_z is much longer than the plasma skin depth $\delta = c/\omega_{pe}$, where c is the speed of light and $\omega_{pe} = \sqrt{n_{pe}e^2/m_e\varepsilon_0}$ is the plasma electron angular frequency (with n_{pe} the plasma electron density, e the elementary charge, m_e the electron mass at rest, and ε_0 the vacuum permittivity), wakefields act on the bunch itself. When the bunch rms transverse size $\sigma_{r0} \lesssim \delta$, the axisymmetric mode of the transverse two-stream instability (TTSI) [4,5], i.e., the self-modulation instability (SMI) [6–9], can take place. SMI longitudinally modulates the density of the bunch along its axis with wave number $k = k_\parallel = \delta^{-1}$. The resulting microbunch train then resonantly drives large-amplitude wakefields that can be used for particle acceleration, as in the AWAKE experiment at CERN [7,8,10,11].

When $\sigma_{r0} > \delta$, the plasma return current can flow within the bunch. When the peak bunch to plasma electron density ratio $n_{b0}/n_{pe} \sim 1$ and the Lorentz factor of the bunch $\gamma \sim 1$, repulsion between opposite currents tends to reinforce any transverse anisotropy in the current density distributions, possibly leading to the development of the current filamentation instability (CFI) [3,12]. This instability modulates the bunch transversely ($k = k_\perp$) into multiple filaments, which self-pinch to transverse size of the order of δ [12] and with a higher current density than that of the incoming bunch. Calculations and numerical simulation results show that a wide spectrum of wave numbers is excited [12–15]. The occurrence of CFI generates magnetic fields within the medium, thus converting part of the kinetic energy carried by streaming particles into magnetic energy [16–18]. This process is, in fact, one of the plausible candidates for the magnetization of astrophysical media [19,20], as well as for the magnetic field enhancement that could explain phenomena such as long-duration afterglow of gamma-ray bursts [21,22] and collisionless shocks [23]. It also plays an important role in the transport and deposition of energy by hot electrons in inertial confinement fusion targets [24,25]. Previous experiments using electron bunches [26–28] investigated conditions where the instability reached saturation and filaments even started merging with each other, a process first described in [29]. The effect of the return current on the focusing of an electron bunch was observed in a passive plasma lens with $\sigma_{r0} \gtrsim \delta$ [30]. CFI is an unwanted instability for effective plasma wakefield excitation because it would degrade the structure of the wakefields and therefore the emittance of the accelerated bunch.

Theory [3,14,31] and numerical simulation results [32,33] show that in the case of relativistic ($\gamma \gg 1$), wide, long ($\sigma_z/\delta > 1$), and underdense ($n_{b0}/n_{pe} \ll 1$) bunches, the oblique two-stream instability (OTSI) is the dominant process. In this case, the wave number retains perpendicular and parallel components: $\vec{k} = \vec{k}_\perp + \vec{k}_\parallel$. OTSI thus tends to generate finite-length filaments surrounded by the return current of plasma electrons moving nonrelativistically with speed $v_e \sim (n_{b0}/n_{pe})c \ll c$. In the following, we thus refer to this phenomenon with the general term *filamentation*.

Using a long, relativistic proton (p^+) bunch, we perform experiments, in the context of AWAKE, in the very underdense ($n_{b0}/n_{pe} \leqslant 10^{-2}$) and very relativistic ($\gamma_p = 427$) regime. Protons have mass $m_p \sim 1836\, m_e$, increasing the inertia ($\gamma_p m_p$) of the bunch particles and slowing the growth of instabilities, when compared to the most described case of an electron bunch with $\gamma < 117$. OTSI is therefore expected to be the dominant instability. Both bunch (relative energy spread $\sim$0.2%) and plasma (electron temperature $\sim$few eV) can be considered as cold. The growth rate of OTSI is given by

$$\Gamma = \frac{\sqrt{3}}{2^{4/3}}\left(\frac{n_{b0}m_e}{n_{pe}m_p\gamma_p}\right)^{1/3}\omega_{pe} = \Gamma_e\left(\frac{m_e}{m_p}\right)^{1/3}, \qquad (1)$$

where Γ_e is the growth rate for the case of an infinitely long, uniform beam [3].

In this paper, we show with experimental results that when $\sigma_{r0}/\delta \geqslant 1.5$ and $\sigma_z/\delta > 1$, OTSI, and therefore filamentation, occurs. We observe the presence of filaments on transverse time-integrated images of the bunch after propagation through 10 m of plasma. Time-resolved images of a transverse slice of the bunch indicate that filaments become observable only late along the bunch, consistent with the early stage of OTSI and with the spatiotemporal nature of filamentation of a finite-length bunch [32–36]. We observe that for $\sigma_{r0}/\delta = 1.5$, and without observable differences in the incoming time-integrated bunch charge density distribution, the outcome of the experiment alternates between filamentation (evidenced by transverse modulation) and SMI (evidenced by longitudinal modulation). For values below this threshold, SMI always takes place and filamentation is not observed from time-integrated images of the bunch. We give a rough estimate the amplitude of the magnetic field generated by the occurrence of filamentation. We calculate that the amount of magnetic energy converted from kinetic energy is small, but increases with the plasma electron density due to an increase of the number of filaments in a larger area of the bunch.

II. EXPERIMENTAL SETUP

The plasma (see Fig. 1) is generated by a DC-pulsed discharge in a 10-m-long, 25-mm-diameter, cylindrical glass tube filled with argon at pressure 23.8 Pa [37]. The plasma fills the entire diameter of the tube. The peak discharge current used for these experiments is $\sim$500 A, with a pulse duration of $\sim$25 μs.

The 43 nC bunch with normalized emittance $\epsilon_N = 2.5$ mm mrad composed of 400 GeV/c p^+ is delivered by the CERN Super Proton Synchrotron. By varying the delay between the p^+ bunch arrival time and the start of the discharge between 25 and 200 μs, we vary the plasma electron density between $n_{pe} = 9.38$ and 0.68×10^{14} cm^{-3}, respectively, and thus the value of σ_{r0}/δ (σ_{r0} constant), due to recombination of the plasma. The values of n_{pe} as a function of delay were measured offline by longitudinal double-pass interferometry

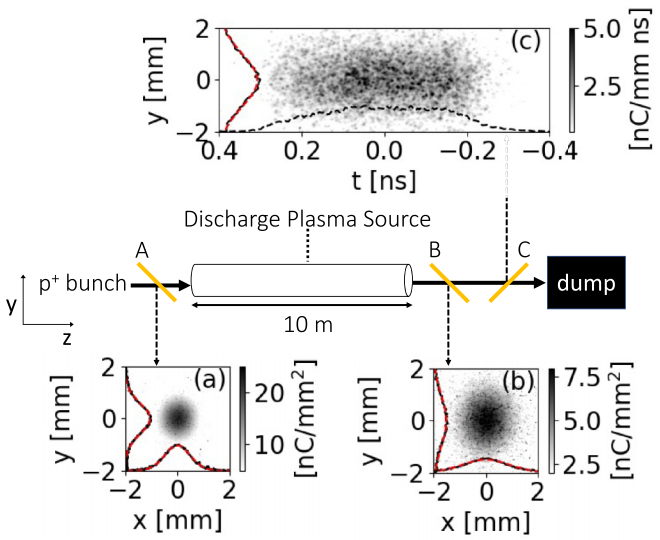

FIG. 1. Schematic of the AWAKE experimental setup (not to scale). Insets: Typical images of the bunch with neither plasma nor gas in the source. (a), (b) Transverse time-integrated images of the bunch at screens A and B, respectively. (c) Time-resolved image at screen C. Solid black lines in the insets: Transverse projections of the distributions. Red dashed lines: Gaussian fits of the transverse projections. Dashed black line in inset (c): Longitudinal projection.

[38] and, in these experiments, from the frequency of the microbunch train resulting from SMI, with bunches with small transverse size ($\sigma_{r0} \sim 0.2$ mm) such that $\sigma_{r0}/\delta < 1$ [7].

We measure the bunch current density distribution using aluminum-coated silicon wafers placed at 45° in the beam path, emitting optical transition radiation (OTR) when protons enter them. Backward OTR is imaged onto the chips of CMOS cameras (screens A, B, and C; Fig. 1) to obtain transverse, time-integrated images of the bunch. The light produced by screen C is also sent to the entrance slit of a streak camera, producing time-resolved images of the bunch. Insets (a), (b), and (c) in Fig. 1 show the corresponding images of the p^+ bunch while neither gas nor discharge are present in the source.

For the measurements presented here, we employ beam optics providing a bunch transverse size that is larger than that normally used for wakefield acceleration and SMI experiments (i.e., $\sigma_{r0} > 0.2$ mm) [9]. We perform Gaussian fits (red dashed lines) on the transverse projections (black solid lines) to determine the rms transverse size $\sigma_{x,y}$ of the bunch at the various screens. We measure $\sigma_{x,y} = (0.45, 0.54) \pm 0.01$ mm (the uncertainty corresponds to the standard deviation of 20 consecutive events) at screen A, ∼1.3 m upstream of the plasma entrance. As the difference between sizes in the two transverse planes (x and y) is small and not relevant for the measurements described here, in the following we use the average of the two values, $\sigma_{r0} = 0.50$ mm, to calculate the ratio σ_{r0}/δ. We note here that the beam is diverging entering the plasma.

At screen B, the transverse sizes obtained with the same procedure are $\sigma_{x,y} = (0.80, 0.87) \pm 0.02$ mm ($\sigma_r = 0.84$ mm). This screen is purposely placed as close as possible to the plasma exit (∼0.3 m downstream of it) because we expect filaments with size a fraction of that of the bunch, and likely higher emittance, to strongly diverge while traveling in vacuum from the plasma exit to the screens. Their visibility is therefore expected to decrease with propagation distance. The spatial resolution at screen B is ∼0.027 mm, measured as the 50% modulation of the transfer function. This is much smaller than the expected transverse size of the filaments: for the maximum density used in these experiments, $n_{pe} \leqslant 9.38 \times 10^{14}$ cm^{-3}, $\delta \geqslant 0.17$ mm.

We note here that images of the bunch before and after the source are Gaussian and smooth, i.e., they show no features at the expected scale size of the filaments (∼δ). The images at screen A therefore provide a good representation of the transverse charge density distribution and size of the bunch entering the source, for every event, with and without plasma.

Screen C is positioned ∼3.5 m downstream of the plasma exit. Thus, narrow features of the bunch (i.e., filaments) leaving the plasma with large divergence may not be as clearly recognizable on time-resolved images as on time-integrated ones at screen B. We measure the bunch duration $\sigma_t = (163 \pm 3)$ ps as the rms of the longitudinal projection of time-resolved images with no gas in the source [black dashed line on Fig. 1(c)]. Therefore, $\sigma_z = \sigma_t c \gg \delta$ and $n_{b0} = 1.3 \times 10^{12}$ cm$^{-3} < 10^{-2}\, n_{pe}$ at the plasma entrance for all measurements presented here.

III. EXPERIMENTAL RESULTS

Figures 2(a)–2(d) show four, single-event, time-integrated images of the p^+ bunch at the screen close to the plasma exit (screen B, Fig. 1) after propagation in plasma with $n_{pe} = 9.38 \times 10^{14}$ cm^{-3}, and thus $\sigma_{r0}/\delta = 2.9$. All images show clear evidence of filaments within a radius in the bunch $r \sim 0.5$ mm $< \sigma_r = 0.79$ mm, while the overall Gaussian distribution of the bunch is maintained, as indicated by the horizontal lineouts (black lines, lineouts chosen along the dashed gray lines to evidence the presence of filaments). This indicates that beyond a given radius of the bunch, the charge density and growth rate are not large enough for filamentation to develop over 10 m of plasma. The rms size of a typical filament, such as the one indicated by the red arrow in Fig. 2(a), is ∼0.12 mm, and the distance between neighboring filaments as those indicated by the red bracket is ∼0.27 mm. These values are commensurate with $\delta = 0.17$ mm, as expected from filamentation (OTSI or CFI) [28]. The spaces between filaments correspond to regions where plasma return current flows [12]. A hollow ring of bunch charge centered on a filament is, for example, clearly visible in Fig. 2(c) (indicated by the red arrow).

Because the transverse component of the instability grows from nonuniformities in the transverse distribution of the bunch and return current densities ($k = k_\perp$), the location, shape, and number of the filaments change from event to event with no recognizable pattern in the incoming distribution [monitored with screen A; images not shown, but similar to Fig. 1(a)]. The instability took place on all 64 events of the dataset, as evidenced by clear signs of filaments on every image (see Supplemental Material [39]).

Figure 3 shows the time-resolved image of the entire p^+ bunch (traveling from left to right), obtained at screen C,

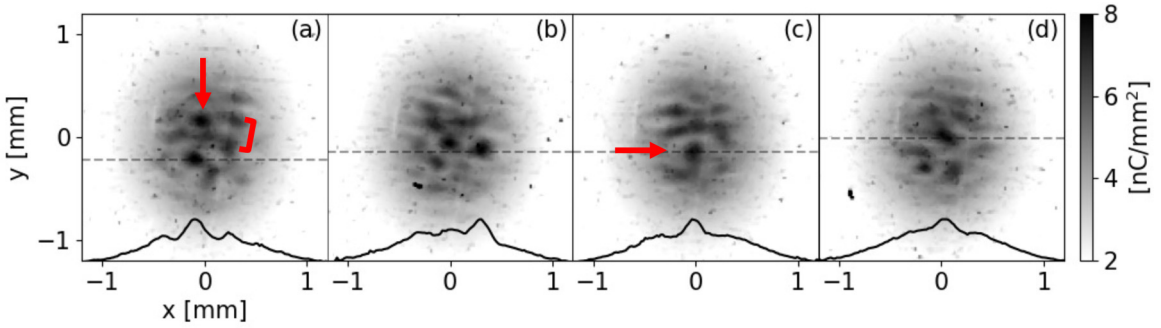

FIG. 2. Transverse, time-integrated, single-event images of the p^+ bunch after propagation in plasma at screen B (see Fig. 1) with $n_{pe} = 9.38 \times 10^{14}$ cm^{-3} and $\sigma_{r0}/\delta = 2.9$. Black lines: Lineouts along the corresponding dashed gray lines. Color map and lineouts chosen to enhance the visibility of the filaments ($\geqslant$2 nC/mm^2).

corresponding to the event of Fig. 2(b). For $t < 0.2$ ns (i.e., over most of the bunch duration), the transverse distribution (dashed black line shows the transverse projection around the gray dashed line, for $-0.1 < t < -0.06$ ns) remains essentially Gaussian as in the case with no plasma [dashed red line shows the transverse projection of Fig. 1(c) around the same time along the bunch], with no sign of occurrence of SMI or OTSI (filaments). In the case of SMI, the transverse distribution would widen along the bunch, forming a halo around the microbunch train [9,40]. This absence of SMI is confirmed by Fourier analysis of the longitudinal bunch density distribution (see below) and is in agreement with previous results that we reported in [9], showing that when increasing the size of the $\sigma_{r0} \sim 0.2$ mm bunch, which always experiences SMI, to $\sigma_{r0} \sim 0.5$ mm (as in this experiment) while keeping n_{pe} constant, SMI no longer develops. This occurs because increasing σ_{r0} decreases the bunch density ($\propto \sigma_{r0}^{-2}$), and therefore also decreases the amplitude of the initial wakefields from which SMI can grow. The resulting focusing force from noise wakefields becomes too small to overcome the natural divergence of the bunch due to its emittance.

Even though filaments strongly diverge before reaching screen C (their relative size becomes much larger than at screen B, as seen on time-integrated images at screen C; see

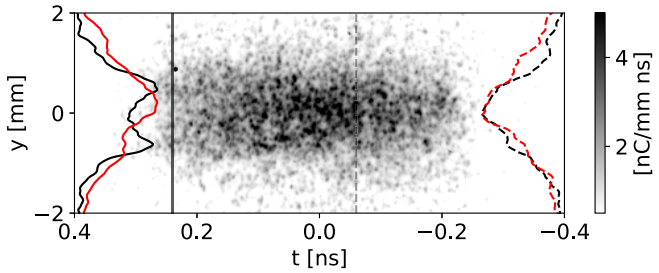

FIG. 3. The ns-scale, time-resolved, single-event image at screen C (see Fig. 1) for the event (b) of Fig. 2. $n_{pe} = 9.38 \times 10^{14}$ cm^{-3}, $\sigma_{r0}/\delta = 2.9$. Front of the bunch at $t < 0$. Black dashed and continuous lines: transverse projection for $-0.1 < t < -0.06$ ns (front of the bunch, along the dashed gray line) and $0.24 < t < 0.28$ ns (back of the bunch, along the continuous gray line), respectively. Red lines: Transverse projections of Fig. 1(c), for the same t along the bunch.

Supplemental Material [39]), the transverse distribution in the back of the bunch (continuous black line shows the transverse projection along the gray continuous line, for $0.24 < t < 0.28$ ns) shows evidence of splitting of the distribution within that time slice, consistent with the formation of two filaments in the back of the bunch. For comparison, we show a projection for the case with no plasma [Fig. 1(c)] for the same time slice (continuous red line). This late occurrence along the bunch is consistent with the only partial density modulation observed on time-integrated images and on their transverse distributions (Fig. 2).

We note here that time-resolved images show a less clear evidence of filamentation than the time-integrated ones (see Supplemental Material [39] for the entire dataset). This is because the streak camera only captures a transverse slice of the p^+ bunch (similar to a smeared-out version of the lineouts shown in Fig. 2) and because the optical system has a limited spatial resolution $O(200\ \mu\text{m})$. To obtain the best time resolution, we choose a 80-μm-wide slice through the center of the bunch. Thus, filaments can only be observed when they form within the direction of the slice.

This observation provides an indication of the spatiotemporal nature of filamentation of a bunch with finite duration, as observed in simulations [33,35,36] and shown in theory [12,14,15], but not in previous experiments with a short electron bunch [28]. It is also consistent with the reduced growth of a finite-length, diverging bunch with respect to that of a uniform, infinitely long, collimated beam [32,33]. We therefore observe the result of the early stage of OTSI.

As discussed in [9], decreasing n_{pe}, while keeping σ_{r0} constant, increases the amplitude of the initial wakefields because the fraction of the p^+ bunch charge contained within δ increases. Moreover, when σ_{r0}/δ approaches unity, the plasma return current starts flowing outside of the bunch, favoring focusing into a single "filament" [30] and (in the case of a long bunch, i.e., $\sigma_z/\delta > 1$) the development of SMI over that of filamentation. In this experiment, we consistently observe the occurrence of filamentation (transverse modulation with no longitudinal modulation) also on all events with plasma densities $n_{pe} = 7.37$ and 5.82×10^{14} cm^{-3}, corresponding to $\sigma_{r0}/\delta = 2.5$ and 2.3.

When decreasing n_{pe} further to 2.25×10^{14} cm^{-3}, thus σ_{r0}/δ to 1.5, features on time-integrated images obtained

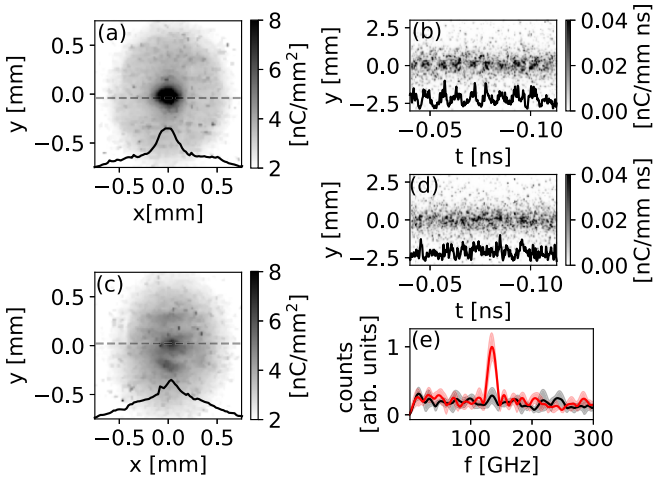

FIG. 4. (a), (c) Transverse, time-integrated, single-event images of the p^+ bunch at screen B (see Fig. 1) after propagation in plasma with $n_{pe} = 2.25 \times 10^{14}$ cm^{-3}, $\sigma_{r0}/\delta = 1.5$. Black lines: Lineout along the corresponding dashed gray lines. (b), (d) The ps-scale, time-resolved, single-event images at screen C, corresponding to (a) and (c), respectively. Black lines: On-axis longitudinal distributions obtained by summing counts over $-0.217 \leqslant y \leqslant 0.217$ mm. (e) Average power spectra from DFT of on-axis distributions of single-event images [as in (b) and (d)]. Average amplitude of the distributions subtracted to remove the peak at $f = 0$. Red line: Average of the power spectra of 20 events showing a single "filament" on screen B [e.g., (a)]. Black line: Average of the power spectra of 23 events showing multiple filaments on screen B [e.g., (c)]. Shaded areas show the extent of the rms variations over the events.

at screen B alternate between events with one, on-axis "filament" [Fig. 4(a)] and events with multiple filaments [Fig. 4(c)]. For 43 consecutive events collected at this density, 20 show one on-axis "filament" and 23 show multiple filaments, indicating an almost even alternation.

When only one filament occurs, time-resolved images at screen C [e.g., Fig. 4(b), ps scale] show a microbunch train (i.e., longitudinal modulation of the density all along the bunch), and the on-axis longitudinal distributions [black line in Fig. 4(b)] exhibit a periodic modulation, indicating that SMI has taken place. The average of the power spectra obtained from discrete Fourier transform (DFT) analysis of the longitudinal distributions of single-event images, for the 20 cases when the time-integrated images show only one filament, is shown in Fig. 4(e) (red line, the shaded area represents the rms variation). The spectrum has a clear peak at $f_{\rm mod} = 135 \pm 1$ GHz (the uncertainty is the standard deviation of the measured values), in agreement with the value of the plasma electron frequency $f_{pe} = \omega_{pe}/2\pi = 135 \pm 5$ GHz (the error corresponds to the uncertainty on the interferometric measurement [38]), as typical of SMI [7]. This is consistent with the transverse distribution of Fig. 4(a) (black line shows the lineout along the dashed gray line) showing a bright core and wide halo, corresponding to the microbunch train and to the defocused protons, respectively [8].

Conversely, the average power spectrum of the images for the 23 events with multiple filaments [black line in Fig. 4(e)] does not have any peak above the noise level, consistent with the distribution of Fig. 4(d) showing no particular periodicity, i.e., no detectable occurrence of longitudinal modulation (SMI or OTSI) along the core of the bunch. In this case, filaments occur within a radius of the bunch $r \sim 0.25$ mm, smaller than in the higher n_{pe} and smaller δ case (Fig. 2). The transverse modulation also appears less deep than at higher densities.

These results indicate that the parameters of the experiment are such that over the 10-m-long plasma, filamentation grows to an observable level, only late along the bunch (Fig. 3), when $\sigma_{r0}/\delta > 1.5$, and no periodic modulation develops, as shown with SMI in [9]. When $\sigma_{r0}/\delta = 1.5$, we observe multiple filaments only when SMI does not develop [Figs. 4(c) and 4(d)]. When it occurs, SMI grows to a significant level over most of the bunch (starting from its front) [9,40] and thus dominates over the possible filamentation. Indeed, the formation of a fully modulated bunch train is an indication that SMI reached (or is close to) saturation all along the bunch, whereas OTSI has barely grown (in contrast, for example, to what was observed in [28]). When filamentation occurs, it develops only late along the bunch and we observe that it splits the bunch charge among short filaments, but we detect no longitudinal component of modulation. Since neither the initial perturbation (e.g., noise) that the instabilities grow from nor their growth rate are measured, only their combination (exponentiation of the initial level), we can only conclude that in our experiments, this combination is much smaller for OTSI than for SMI. We also expect the divergence of the beam at the plasma entrance to generally decrease the growth of the instabilities that could develop (SMI and OTSI) [9,32].

The fact that we do not observe longitudinal modulation in the conditions where filamentation occurs (see Figs. 3, 4 and Ref. [9]) indicates that the effect of the longitudinal component ($k_\parallel$) of OTSI is much smaller than the effect of the transverse component ($k_\perp$), possibly also in agreement with the early stage of the instability. We also note that longitudinal components of OTSI recorded in, e.g., two filaments on the time-resolved images would have the same frequency but likely different relative phases, which would lower the amplitude of the corresponding peak in the DFT average power spectrum, making detection more difficult. We therefore calculate the amplitude of the magnetic fields generated by OTSI as only due to the filamentation we observe.

When filamentation grows, the total net current and magnetic field remain zero on average, but the formation and pinching of the filaments with higher current density than that of the bunch without filaments, and the expulsion of the return current, generate a net local magnetic field. Since, at the early stage of filamentation, the overall Gaussian transverse distribution of the bunch is preserved, we use the time-integrated images from screen B [e.g., Figs. 2(a)–2(d)] to estimate the magnetic field generated by the bunch-plasma interaction. We generate the distribution of the return current as the complementary of the bunch current density two-dimensional distribution with respect to the underlying smooth bunch distribution, so that the total current is zero. The smooth distribution is obtained by applying a median filter of size $(0.38\ \text{mm})^2$, larger than the transverse size of the filaments for all cases in these measurements, to the time-integrated images of the bunch after propagation in plasma. We use this smoothed distribution and not the

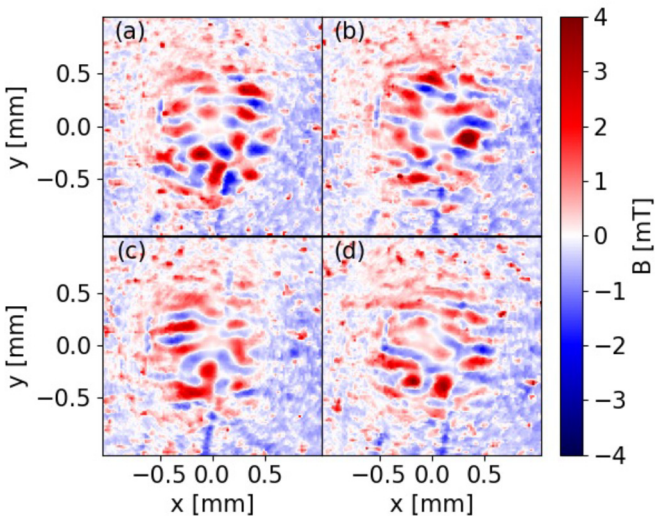

FIG. 5. Magnitude of the transverse magnetic field calculated from the images in Figs. 2(a)–2(d). $n_{pe} = 9.38 \times 10^{14}$ cm^{-3} and $\sigma_{r0}/\delta = 2.9$.

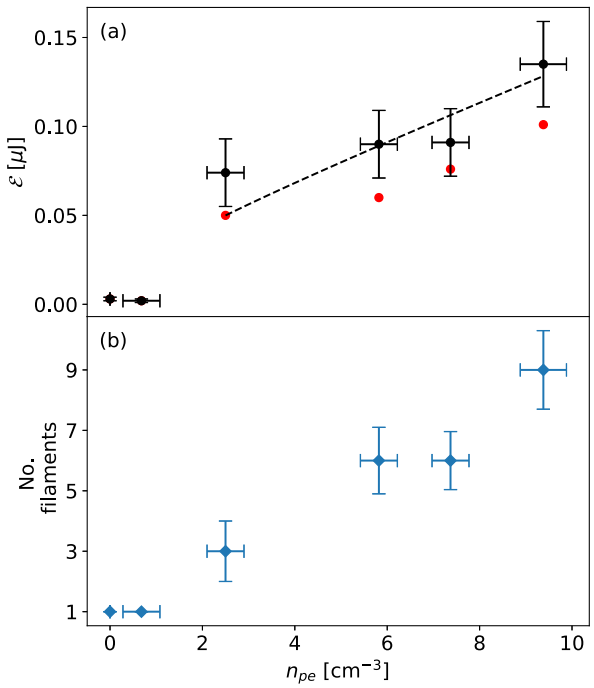

FIG. 6. (a) Magnetic energy within the bunch volume as a function of n_{pe}. Black symbols: Average of consecutive images; error bars show the rms variation over the events in each dataset. Dashed line: Result of the fit with function $\propto \exp(n_{pe}^{1/3})$ to the cases where filamentation occurs. Red symbols: Minimum value for each value of n_{pe}. (b) Average number of filaments within transverse, time-integrated images at screen B; error bars show the rms variation over the events in each dataset. For $n_{pe} = 2.25 \times 10^{14}$ cm^{-3}, only events showing multiple filaments (see Fig. 4) are considered.

plasma off one because of the global focusing that the bunch experiences along the plasma [41]. We then use Ampère's law to calculate the amplitude of the transverse magnetic field due to filamentation as the sum of the fields generated by the two current densities. To calculate the current density in each pixel of the images, we use the bunch charge density (see Figs. 2 and 4) divided by the bunch duration σ_t (even though filaments appear only late along the bunch). This procedure allows us to obtain a rough estimate of the magnetic field averaged over the bunch duration.

Figures 5(a)–5(d) show maps of the magnitude of the magnetic field calculated from Figs. 2(a)–2(d). The magnetic field is maximum positive (convention) at the locations of the bunch filaments (red areas), changes sign around them (blue areas), and vanishes on average outside of the bunch because, by construction, the plasma return current globally shields the magnetic field of the bunch, but does not shield it locally, i.e., at the scale of the size of the filaments ($\sim\delta$). The magnetic field at the center of the filaments is not zero because of the fact that the filaments are not perfectly axisymmetric and they are surrounded by other nonaxisymmetric filaments and because of the finite resolution of the diagnostics. The amplitude of the magnetic field reaches $\sim$4 mT. We note that this field amplitude is sufficient to bend the trajectory of a 400 GeV/c proton by δ over the plasma length to form filaments. We also note that the maximum transverse magnetic field generated by the low-current ($\sim$50 A) bunch at the peak of its density [$t = 0$, Fig. 1(c)] is $\sim$30 mT. Therefore, even these late filaments generate fields with magnitude comparable to that of the incoming bunch in vacuum.

We calculate the amount of magnetic energy within the bunch as $\mathcal{E} = \int dV < B^2 > /2\mu_0$, where $V = (2\pi)^{3/2}\sigma_r^2 c\sigma_t$ is the bunch volume with σ_r the transverse size at screen B. Figure 6(a) shows that the average magnetic energy (black symbols) increases with n_{pe} and reaches $\sim$0.13 μJ for $n_{pe} = 9.38 \times 10^{14}$ cm^{-3}. The error bars, representing the rms variation over the >20 events at each density, are relatively wide. This is consistent with the instability nature of the process, producing different numbers of filaments with different current densities and distributions for every event (see Supplemental Material [39]). Since filaments are produced for every event, the minimum energy (red symbols) at each density also increases with n_{pe}.

The increase of the magnetic energy with n_{pe} is due to the increase of the maximum amplitude of the magnetic field. The dashed line in Fig. 6(a) shows the result of a fit to the experimental data where filamentation occurs with a function $\propto B^2(z) \propto \exp(2\Gamma z/c) \propto \exp(n_{pe}^{1/3})$. The result of the fit shows a fairly good agreement with the data, and it is consistent with the (slow) increase of the magnetic field and energy with plasma electron density. The increase in magnetic energy is also due to the increase in the number of filaments developing within the bunch [Fig. 6(b)]. This is consistent with the radius over which filaments are observed in time-integrated images [$r \sim 0.5$ mm in Fig. 2 and $r \sim 0.25$ mm in Fig. 4(c)], and with the transverse modulation depth.

The small (compared to the total kinetic energy of the bunch, $\sim$17 kJ) amount of magnetic energy shown in Fig. 6(a) is consistent with the late development of the instability along the bunch (Fig. 3), with the short length of the interaction and with the low current and current density of the incoming bunch. Along the earlier part of the bunch, the two currents compensate for each other, and both the amplitude of the

magnetic field and the corresponding magnetic energy are close to zero.

IV. CONCLUSIONS

The experimental results presented here show that a long, underdense, relativistic p^+ bunch propagating in plasma undergoes the oblique instability when its transverse size σ_{r0} is larger than ∼1.5 plasma skin depth. This is evidenced by the formation of higher-current-density filaments, transversely modulating the bunch density and current density. This can be compared to previous experimental results where the measured threshold for CFI was $\sigma_{r0} \sim 2.2$ plasma skin depth [28]. They both confirm the expectation of filamentation to develop when $\sigma_{r0}/\delta > 1$. We also observe the spatiotemporal nature of OTSI, manifesting itself through its development only late along the bunch in this case. Conversely, and most importantly for future plasma wakefield accelerators, filamentation does not occur when the transverse size is smaller than the plasma skin depth. Instead, and as measured before, the long p^+ bunch undergoes SMI. At threshold and with the parameters of this experiment, the bunch-plasma system alternates between the two instabilities. Our analysis of the results also suggests that filamentation generates magnetic fields in the system, and that the amount of energy converted into magnetic energy increases when increasing the plasma electron density. If the current filamentation or oblique instability of charged particle streams occurred in the universe, they would thus generate the initial magnetic fields that may then be amplified by dynamo processes [42].

ACKNOWLEDGMENTS

P.M., L.V., and E.W. thank A. Bret for fruitful discussions. This work was supported in parts by Fundação para a Ciência e Tecnologia - Portugal (Grants No. CERN/FIS-TEC/0017/2019, No. CERN/FIS-TEC/0034/2021, No. UIBD/50021/2020), STFC (AWAKE-UK, Cockcroft Institute core, John Adams Institute core, and UCL consolidated grants), United Kingdom, and the National Research Foundation of Korea (Grants No. NRF-2016R1A5A1013277 and No. NRF-2020R1A2C1010835). M.W. acknowledges the support of DESY, Hamburg. Support of the Wigner Datacenter Cloud facility through the Awakelaser project is acknowledged. TRIUMF contribution is supported by NSERC of Canada. The University of Wisconsin, Madison, acknowledges support by NSF Award No. PHY-1903316. The AWAKE collaboration acknowledges the SPS team for their excellent proton delivery.

[1] P. Chen, J. M. Dawson, R. W. Huff, and T. Katsouleas, Acceleration of electrons by the interaction of a bunched electron beam with a plasma, Phys. Rev. Lett. **54**, 693 (1985).

[2] B. Lehnert, Experimental evidence of plasma instabilities, Plasma Phys. **9**, 301 (1967).

[3] A. Bret, L. Gremillet, and M. E. Dieckmann, Multidimensional electron beam-plasma instabilities in the relativistic regime, Phys. Plasmas **17**, 120501 (2010).

[4] J. R. Pierce, Possible fluctuations in electron streams due to ions, J. Appl. Phys. **19**, 231 (1948).

[5] D. Bohm and E. P. Gross, Theory of plasma oscillations. A. Origin of medium-like behavior, Phys. Rev. **75**, 1851 (1949).

[6] N. Kumar, A. Pukhov, and K. Lotov, Self-modulation instability of a long proton bunch in plasmas, Phys. Rev. Lett. **104**, 255003 (2010).

[7] E. Adli *et al.* (AWAKE Collaboration), Experimental observation of proton bunch modulation in a plasma at varying plasma densities, Phys. Rev. Lett. **122**, 054802 (2019).

[8] M. Turner *et al.* (AWAKE Collaboration), Experimental observation of plasma wakefield growth driven by the seeded self-modulation of a proton bunch, Phys. Rev. Lett. **122**, 054801 (2019).

[9] L. Verra, S. Wyler, T. Nechaeva, J. Pucek, V. Bencini, M. Bergamaschi, L. Ranc, G. Zevi Della Porta, E. Gschwendtner, P. Muggli *et al.* (AWAKE Collaboration), Development of the self-modulation instability of a relativistic proton bunch in plasma, Phys. Plasmas **30**, 083104 (2023).

[10] P. Muggli *et al.* (The AWAKE Collaboration), AWAKE readiness for the study of the seeded self-modulation of a 400 GeV proton bunch, Plasma Phys. Control. Fusion **60**, 014046 (2018).

[11] AWAKE Collaboration, Acceleration of electrons in the plasma wakefield of a proton bunch, Nature (London) **561**, 363 (2018).

[12] R. Lee and M. Lampe, Electromagnetic instabilities, filamentation, and focusing of relativistic electron beams, Phys. Rev. Lett. **31**, 1390 (1973).

[13] L. O. Silva, R. A. Fonseca, J. W. Tonge, J. M. Dawson, W. B. Mori, and M. V. Medvedev, Interpenetrating plasma shells: Near-equipartition magnetic field generation and nonthermal particle acceleration, Astrophys. J. **596**, L121 (2003).

[14] F. Califano, R. Prandi, F. Pegoraro, and S. V. Bulanov, Nonlinear filamentation instability driven by an inhomogeneous current in a collisionless plasma, Phys. Rev. E **58**, 7837 (1998).

[15] M. Gedalin, M. Medvedev, A. Spitkovsky, V. Krasnoselskikh, M. Balikhin, A. Vaivads, and S. Perri, Growth of filaments and saturation of the filamentation instability, Phys. Plasmas **17**, 032108 (2010).

[16] C. Zhang, J. Hua, Y. Wu, Y. Fang, Y. Ma, T. Zhang, S. Liu, B. Peng, Y. He, C.-K. Huang, K. A. Marsh, W. B. Mori, W. Lu, and C. Joshi, Measurements of the growth and saturation of electron Weibel instability in optical-field ionized plasmas, Phys. Rev. Lett. **125**, 255001 (2020).

[17] C. M. Huntington, F. Fiuza, J. S. Ross, A. B. Zylstra, R. P. Drake, D. H. Froula, G. Gregori, N. L. Kugland, C. C. Kuranz, M. C. Levy, C. K. Li, J. Meinecke, T. Morita, R. Petrasso, C. Plechaty, B. A. Remington, D. D. Ryutov, Y. Sakawa, A. Spitkovsky, H. Takabe *et al.*, Observation of magnetic field generation via the Weibel instability in interpenetrating plasma flows, Nat. Phys. **11**, 173 (2015).

[18] L. Sironi, L. Comisso, and R. Golant, Generation of near-equipartition magnetic fields in turbulent collisionless plasmas, Phys. Rev. Lett. **131**, 055201 (2023).
[19] R. Schlickeiser and P. K. Shukla, Cosmological magnetic field generation by the Weibel instability, Astrophys. J. **599**, L57 (2003).
[20] M. V. Medvedev, L. O. Silva, and M. Kamionkowski, Cluster magnetic fields from large-scale structure and galaxy cluster shocks, Astrophys. J. **642**, L1 (2006).
[21] M. V. Medvedev, D. Lazzati, B. C. Morsony, and J. C. Workman, Jitter radiation as a possible mechanism for gamma-ray burst afterglows: Spectra and light curves, Astrophys. J. **666**, 339 (2007).
[22] M. V. Medvedev, Radiation of electrons in Weibel-generated fields: a general case, Astrophys. Space Sci. **322**, 147 (2009).
[23] M. V. Medvedev and A. Loeb, Generation of magnetic fields in the relativistic shock of gamma-ray burst sources, Astrophys. J. **526**, 697 (1999).
[24] M. Honda, J. Meyer-ter-Vehn, and A. Pukhov, Collective stopping and ion heating in relativistic-electron-beam transport for fast ignition, Phys. Rev. Lett. **85**, 2128 (2000).
[25] L. O. Silva, R. A. Fonseca, J. W. Tonge, W. B. Mori, and J. M. Dawson, On the role of the purely transverse Weibel instability in fast ignitor scenarios, Phys. Plasmas **9**, 2458 (2002).
[26] M. Tatarakis, F. N. Beg, E. L. Clark, A. E. Dangor, R. D. Edwards, R. G. Evans, T. J. Goldsack, K. W. D. Ledingham, P. A. Norreys, M. A. Sinclair, M.-S. Wei, M. Zepf, and K. Krushelnick, Propagation instabilities of high-intensity laser-produced electron beams, Phys. Rev. Lett. **90**, 175001 (2003).
[27] C. M. Huntington, A. G. R. Thomas, C. McGuffey, T. Matsuoka, V. Chvykov, G. Kalintchenko, S. Kneip, Z. Najmudin, C. Palmer, V. Yanovsky, A. Maksimchuk, R. P. Drake, T. Katsouleas, and K. Krushelnick, Current filamentation instability in laser wakefield accelerators, Phys. Rev. Lett. **106**, 105001 (2011).
[28] B. Allen, V. Yakimenko, M. Babzien, M. Fedurin, K. Kusche, and P. Muggli, Experimental study of current filamentation instability, Phys. Rev. Lett. **109**, 185007 (2012).
[29] M. V. Medvedev, M. Fiore, R. A. Fonseca, L. O. Silva, and W. B. Mori, Long-time evolution of magnetic fields in relativistic gamma-ray burst shocks, Astrophys. J. **618**, L75 (2005).
[30] R. Govil, W. P. Leemans, E. Y. Backhaus, and J. S. Wurtele, Observation of return current effects in a passive plasma lens, Phys. Rev. Lett. **83**, 3202 (1999).
[31] A. Bret, Weibel, two-stream, filamentation, oblique, Bell, Buneman...which one grows faster? Astrophys. J. **699**, 990 (2009).
[32] N. Shukla, J. Vieira, P. Muggli, G. Sarri, R. Fonseca, and L. O. Silva, Conditions for the onset of the current filamentation instability in the laboratory, J. Plasma Phys. **84**, 905840302 (2018).
[33] P. San Miguel Claveria, X. Davoine, J. R. Peterson, M. Gilljohann, I. Andriyash, R. Ariniello, C. Clarke, H. Ekerfelt, C. Emma, J. Faure, S. Gessner, M. J. Hogan, C. Joshi, C. H. Keitel, A. Knetsch, O. Kononenko, M. Litos, Y. Mankovska, K. Marsh, A. Matheron *et al.*, Spatiotemporal dynamics of ultra-relativistic beam-plasma instabilities, Phys. Rev. Res. **4**, 023085 (2022).
[34] V. B. Pathak, T. Grismayer, A. Stockem, R. A. Fonseca, and L. O. Silva, Spatial-temporal evolution of the current filamentation instability, New J. Phys. **17**, 043049 (2015).
[35] G. Raj, O. Kononenko, M. F. Gilljohann, A. Doche, X. Davoine, C. Caizergues, Y.-Y. Chang, J. P. Couperus Cabadağ, A. Debus, H. Ding, M. Förster, J.-P. Goddet, T. Heinemann, T. Kluge, T. Kurz, R. Pausch, P. Rousseau, P. San Miguel Claveria, S. Schöbel, A. Siciak *et al.*, Probing ultrafast magnetic-field generation by current filamentation instability in femtosecond relativistic laser-matter interactions, Phys. Rev. Res. **2**, 023123 (2020).
[36] N. Shukla, S. F. Martins, P. Muggli, J. Vieira, and L. O. Silva, Interaction of ultra relativistic fireball beam with plasma, New J. Phys. **22**, 013030 (2020).
[37] N. E. Torrado, N. C. Lopes, J. F. A. Silva, C. Amoedo, and A. Sublet, Double pulse generator for unipolar discharges in long plasma tubes for the awake experiment, IEEE Trans. Plasma Sci. **51**, 3619 (2023).
[38] C. Amoedo *et al.* (AWAKE Collaboration), Demonstration of proton bunch self-modulation in a discharge plasma source (unpublished).
[39] See Supplemental Material at http://link.aps.org/supplemental/10.1103/PhysRevE.109.055203 for the entire dataset with $n_{pe} = 9.38 \times 10^{14}$ cm^{-3} and $\sigma_{r0}/\delta = 2.9$.
[40] L. Verra, G. Zevi Della Porta, J. Pucek, T. Nechaeva, S. Wyler, M. Bergamaschi, E. Senes, E. Guran, J. T. Moody, M. Á. Kedves, E. Gschwendtner, P. Muggli *et al.* (AWAKE Collaboration), Controlled growth of the self-modulation of a relativistic proton bunch in plasma, Phys. Rev. Lett. **129**, 024802 (2022).
[41] L. Verra, E. Gschwendtner, and P. Muggli, Focusing of a long relativistic proton bunch in underdense plasma, arXiv:2302.04051.
[42] A. Brandenburg and K. Subramanian, Astrophysical magnetic fields and nonlinear dynamo theory, Phys. Rep. **417**, 1 (2005).